Journal of Energy Chemistry 51 (2020) 425–433

Contents lists available at ScienceDirect

Journal of Energy Chemistry

journal homepage: www.elsevier.com/locate/jechem

http://www.journals.elsevier.com/journal-of-energy-chemistry/

Critical role of corrosion inhibitors modified by silyl ether functional groups on electrochemical performances of lithium manganese oxides

Min Ji Seong[a,b], Taeeun Yim[a,b,*]

[a] Department of Chemistry, Incheon National University, Yeonsu-gu 22012, Incheon, Republic of Korea
[b] Research Institute of Basic Sciences, College of Natural Science, Incheon National University, Yeonsu-gu 22012, Incheon, Republic of Korea

ARTICLE INFO

Article history:
Received 3 January 2020
Revised 16 February 2020
Accepted 16 February 2020
Available online 26 February 2020

Keyword:
Lithium-ion batteries
Lithium manganese oxide cathode
Electrolyte additive
Corrosion
Silyl ether
Fluoride scavenger

ABSTRACT

Lithium manganese oxides ($LiMn_2O_4$, LMO) have attracted significant attention as important cathode materials for lithium-ion batteries (LIBs), which require fast charging based on their intrinsic electrochemical properties. However, these properties are limited by the rapid fading of cycling retention, particularly at high temperatures, because of the severe Mn corrosion triggered by the chemical reaction with fluoride (F^-) species existing in the cell. To alleviate this issue, three types of silyl ether (Si–O)-functionalized task-specific additives are proposed, namely methoxytrimethylsilane, dimethoxydimethylsilane, and trimethoxymethylsilane. Ex-situ NMR analyses demonstrated that the Si-additives selectively scavenged the F^- species as Si forms new chemical bonds with F via a nucleophilic substitution reaction due to the high binding affinity of Si with F^-, thereby leading to a decrease in the F concentration in the cell. Furthermore, the addition of Si-additives in the electrolyte did not significantly affect the ionic conductivity or electrochemical stability of the electrolyte, indicating that these additives are compatible with conventional electrolytes. In addition, the cells cycled with Si-additives exhibited improved cycling retention at room temperature and 45 °C. Among these candidates, a combination of MTSi and the LMO cathode was found to be the most suitable choice in terms of cycling retention (71.0%), whereas the cell cycled with the standard electrolyte suffered from the fading of cycling retention triggered by Mn dissolution (64.4%). Additional ex-situ analyses of the cycled electrodes using SEM, TEM, EIS, XPS, and ICP-MS demonstrated that the use of Si-additives not only improved the surface stability of the LMO cathode but also that of the graphite anode, as the Si-additives prevent Mn corrosion. This inhibits the formation of cracks on the surface of the LMO cathode, facilitating the formation of a stable solid electrolyte interphase layer on the surface of the graphite anode. Therefore, Si-additives modified by Si–O functional groups can be effectively used to increase the overall electrochemical performance of the LMO cathode material.

1. Introduction

As global warming is becoming a worldwide issue, the demand for environmentally friendly energy sources is increasing. In this context, lithium-ion batteries (LIBs) have been recognized as a promising alternative power source owing to their good cycling performance and moderate rate capability [1–3]. The specification of a cell is significantly affected by the performance of the electrode material, which is related to the specific capacity and working potential, and these mainly depend on the class of electrode materials [4–8]. Therefore, it is important to develop advanced electrode materials that can afford high specific capacities as well as high working potentials during the electrochemical process. In addition, the initial electrochemical performances of the electrode materials should be maintained after long-term cycling.

To date, a range of cathode materials have been proposed, but a limited number of these have been successfully commercialized. For example, lithium cobalt oxide ($LiCoO_2$) was used in the first commercial LIBs owing to its stable cycling performance [9–12], while lithium nickel-cobalt-manganese oxide ($LiNi_xCo_yMn_zO_2$) has been employed to increase the energy density of the cell [13–17], and lithium manganese oxide ($LiMn_2O_4$, LMO) has been applied for task-specific LIB applications that require fast charging of the cell [18–22]. Notably, these cathode materials have similar chemical compositions, i.e., lithium (Li^+), a transition metal (TM), and an oxygen ligand, each of which has an individual role in the electrochemical reaction of the cell. More specifically, Li^+ acts as an ion

* Corresponding author at: Research Institute of Basic Sciences, College of Natural Science, Incheon National University, Yeonsu-gu 22012, Incheon, Republic of Korea.
E-mail address: yte0102@inu.ac.kr (T. Yim).

https://doi.org/10.1016/j.jechem.2020.02.029

carrier between the cathode and anode, the TM (Ni, Co, or Mn) is associated with the electrochemical reaction at the relevant electrochemical potential, and the oxygen ligand stabilizes the metallic components present in the cathode structure. However, these cathode materials are easily degraded under the repeated charging/discharging processes taking place within the cell. In some surface reactions, electrolyte decomposition occurs, resulting in rapid fading of the cycling retention due to the decomposed adducts accumulating on the surface of the cathode disturbing Li^+ migration at the interface between the electrode and the electrolyte, thereby increasing the internal resistance of the cell [23–25]. In addition, as the electrolyte decomposes, it forms fluoride ions (F^-) in the cell, which readily erode the TMs from the cathode structure [26–28]. Notably, F^- is nucleophilic and has a high binding affinity toward the electrophilic TMs, resulting in the dissolution of TMs into the electrolyte. When the TMs dissolve in the electrolyte, irreversible cathode deformation takes place, and the kinetics of Li^+ are hindered at the interface between the anode and electrolyte. If the dissolved TMs diffuse to the surface of the anode in the charging process, these can be easily reduced on the surface, leading to the formation of reduced TM components. In this case, it is difficult to obtain a uniform and stable solid electrolyte interphase (SEI) layer on the anode surface (which is responsible for the stable long-term cycling of the anode), and this triggers rapid fading of the cycling retention of the anode materials. It is therefore important to reduce TM dissolution in the cell to improve the performances of LIBs.

Thus, we herein propose an efficient method to reduce TM dissolution in cells by employing silyl ether (Si–O)-functionalized organic additives, such as methoxytrimethylsilane (MTSi), dimethoxydimethylsilane (DDSi), and trimethoxymethylsilane (TMSi) (Fig. 1a). These additives contain the Si–O functional group, and each additive has a different number of Si–O functional groups in its main skeleton. As Si exhibits a high binding affinity toward F^- [29–32], it is anticipated that these additives can effectively decrease the F^- concentration in the cell via a chemical scavenging reaction between the additives and F, resulting in improved electrochemical performances for the cathode and anode. In addition, studies investigating different derivatives of these additives (i.e., based on the number of Si–O functional groups in the structure) can be useful for understanding the task-specific role of the Si–O functional group, not only in terms of the electrochemical performance, but also in terms of the reaction mechanism. Based on these strategies, three types of additives are evaluated with the LMO cathode material, which is well-known for its limitations, including significant deterioration of the cathode material upon TM dissolution [33–37]. Finally, the relationship between the chemical reactivity of the additive and electrochemical performance of the LMO cathode is systematically investigated.

2. Experimental

Linear sweep voltammetry (LSV) measurements of the electrolytes were performed as follows. Stainless steel was used as the working electrode and Li metal was used as the counter and reference electrodes (three-electrode cell). The standard electrolyte was composed of ethylene carbonate and ethyl methyl carbonate (1:2 v%) with 1.0 M lithium hexafluorophosphate ($LiPF_6$; Panax-Etec), and thereafter, MTSi (TCI), DDSi (Sigma-Aldrich), and TMSi (Sigma-Aldrich) were added to the standard electrolyte. Following fabrication of the three-electrode cells, the potential was increased from the open circuit potential to 5.0 V (vs. Li/Li^+) with a scan rate of 1 mV s^{-1}.

To elucidate the chemical reactivities of the Si-additives with F^- species, tetrabutylammonium fluoride (TBAF, TCI) was added to a plastic bottle and the different Si-additives were added. The

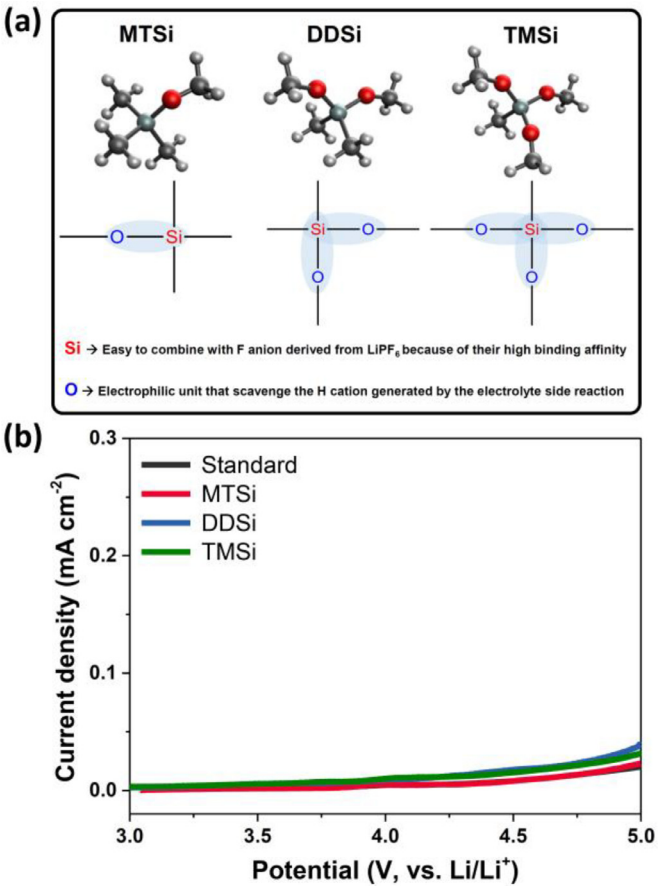

Fig. 1. (a) Molecular structures of MTSi, DDSi, and TMSi, (b) LSV results for standard electrolyte (black), MTSi-containing electrolyte (red), DDSi-containing electrolyte (blue), and TMSi-containing electrolyte (green).

resulting mixtures were stirred for 24 h at room temperature to allow the chemical reaction to occur. After this time, the resulting solutions were analyzed by ^1H and ^{19}F nuclear magnetic resonance (NMR, Bruker) spectroscopy to confirm any modifications in the chemical structures of the Si-additives. Acetone-d_6 was used as the NMR solvent because the solvent peak did not overlap with the data for either TBAF or the Si-additives.

To evaluate the electrochemical performance, the LMO cathode was prepared as follows. A mixture of LMO (Ecopro, active material), poly(vinylidene fluoride) (Kurea, binder), and carbon (Super P, conducting agent) was dispersed in *N*-methylpyrrolidone (Sigma-Aldrich) and finely agitated for at least 1 h. The resulting slurries were then cast onto an Al current collector and dried overnight at 120 °C in an oven, followed by vacuum drying at 120 °C for 12 h. The electrode loading was approximately 7.00 ± 0.07 mg cm^{-2}. The 2032 coin cells were then assembled using the LMO cathode, a Li metal anode, a poly(propylene)/poly(ethylene)/poly(propylene) separator (Celgard), and an electrolyte. The cells were charged/discharged from 3.0 V (vs. Li/Li^+) to 4.3 V (vs. Li/Li^+) at a rate of 0.1 C (1.0 C = 100 mA g^{-1}) for the formation step (two cycles), and then the charging/discharging rate was increased to 1.0 C for 100 cycles at room temperature or 45 °C.

After completion of the cycling steps, each cell was disassembled in an Ar-filled glove-box, and both the LMO cathode and the graphite anode were recovered. The cycled electrodes were then quickly washed with fresh dimethyl carbonate prior to analysis. The particle strength of the cycled LMO cathode material was determined using a microindentor (DUH-211, Shimadzu). The

particles were finely dispersed on the sample station and the probe of the microindentor was placed on the top of the particle. The height of the particle was recorded as a function of the external force. The surfaces of the cycled electrodes were also analyzed using scanning electron microscopy (SEM, JEOL) and transmission electron microscopy (TEM, FEI). The chemical compositions of the cycled electrodes were further elucidated by X-ray photoelectron spectroscopy (XPS, K alpha), and the internal resistances of the cells charged to 4.3 V (vs. Li/Li^+) were determined by electrochemical impedance spectroscopy (EIS) with an AC signal at an amplitude of 10 mV over a frequency range of 10 mHz to 1 MHz using an electrochemical workstation (Zive MP1, WonATech). Finally, the dissolved Mn components were quantified by inductively coupled plasma-mass spectroscopy (ICP-MS, Bruker).

3. Results and discussion

The electrochemical oxidation stabilities of the Si-additives were examined by LSV to determine their task-specific roles in the electrochemical charging/discharging process (Fig. 1b). MTSi, DDSi, and TMSi-containing electrolytes exhibited similar electrochemical behaviors (i.e., oxidation behaviors) to the standard electrolyte. This indicates that the MTSi, DDSi, and TMSi additives are stable under anodic polarization in the usual charging range, i.e., in contrast to typical cathode additives, they do not participate during the formation of cathode-electrolyte interphases through an electrochemical oxidation reaction, but act only as F^- scavengers in the cell [38]. In addition, it was found that the addition of Si-additives to the electrolyte slightly decreased the ionic conductivities of the electrolytes (standard electrolyte: 10.60 mS cm^{-1}, 0.25 MTSi-electrolyte: 9.60 mS cm^{-1}, 0.25 DDSi-electrolyte: 9.27 mS cm^{-1}, and 0.25 TMSi-electrolyte: 8.73 mS cm^{-1}) (Fig. S1). It should be noted that size of the additive molecule also significantly affects the ionic conductivity of the electrolyte, whereby the ionic conductivity of the electrolyte decreases upon increasing the additive size (MTSi < DDSi < TMSi) due to increased disturbance of Li^+ migration with increased additive steric hindrance. In addition, the amount of additives also affected the ionic conductivity of the electrolyte, with a gradual decrease being observed upon increasing the additive amount (standard electrolyte: 10.60 mS cm^{-1}, 0.25 MTSi-electrolyte: 9.60 mS cm^{-1}, 0.50 MTSi-electrolyte: 9.40 mS cm^{-1}, and 1.00 MTSi-electrolyte: 9.15 mS cm^{-1}). In the case of the DDSi and TMSi additives, similar physicochemical behaviors were observed (0.25 DDSi-electrolyte: 9.27 mS cm^{-1}, 0.50 DDSi-electrolyte: 8.95 mS cm^{-1}, and 1.00 DDSi-electrolyte: 8.66 mS cm^{-1}; 0.25 TMSi-electrolyte: 8.73 mS cm^{-1}, 0.50 TMSi-electrolyte: 8.56 mS cm^{-1}, and 1.00 TMSi-electrolyte: 8.12 mS cm^{-1}). Importantly, the Si-additive-containing electrolytes continued to exhibit compatible ionic conductivities to allow the facilitation of Li^+ migration between the electrodes in the LIBs [39–42].

The F^--scavenging performances of the Si-additives were then elucidated by ex-situ NMR studies (Fig. 2a). More specifically, the Si-additives were initially reacted with TBAF (which is equivalent to F^- based on their similar chemical reactivities) [43–45], and the resulting solutions were analyzed by ^1H NMR spectroscopy to confirm modifications of the Si-additive molecular structures. Indeed, in the ^1H NMR spectra, new peaks were observed at 3.27 ppm (singlet) and ~0.00 ppm (singlet) in the presence of the Si-additives, and these distinctive signals corresponded to methanol [46–48] and the fluorinated silane compounds [49–52], respectively. These new peaks provide strong evidence to support the effective scavenging of the F^- species by the Si-additives in the cell. Indeed, the peaks observed at ~0.00 ppm, corresponding to the fluorinated silanes, indicate that Si forms new covalent bonds with F through a nucleophilic substitution reaction between Si and the F^- species (Fig. 2b). In addition, the ^{19}F NMR data show a chemical shift value of −124.3 ppm for the F atoms in TBAF, and this shifts to approximately −115.0 ppm (MTSi: −113.6 ppm, DDSi: −115.0 ppm, and TMSi: −115.7 ppm) after completion of the reaction (Fig. S2). This indicates that the chemical environment of F changes after the reaction between Si and F. Since a nucleophilic substitution reaction involving the F^- species should be accompanied by the formation of an elimination product, it was noted that the new peak observed at 3.27 ppm (corresponding to MeOH) further confirms that this reaction did indeed take place, since MeO^- is the main leaving group, and this then forms MeOH in solution [53,54]. These ex-situ NMR analyses thereby strongly suggest that the Si-additives decrease the F^- concentration in the cell by a selective scavenging reaction, thereby improving the cycling performance of LMO cathode materials.

The electrochemical performances of the Si-additives were then evaluated and the results are presented in Fig. 3. At room temperature, all cells exhibited identical potential profiles in the first charge/discharge cycle, and the initial specific capacities of the cells were similar at ~106.8 mAh g^{-1} (Fig. 3a and b). During cycling retention, the cells cycled with the electrolytes containing the Si-additives exhibited slightly increased retentions compared to that cycled with only the standard electrolyte. In addition, for the cells cycled with the Si-additive-containing electrolytes, the retention of the cell was found to be affected by the amount of additive used in the electrolyte, whereby low amounts of additive were effective in increasing the retention of the cells (MTSi: 97.5% (0.25 wt%) to 92.7% (1.00 wt%), DDSi: 97.0% (0.25 wt%) to 91.4% (1.00 wt%), and TMSi: 96.2% (0.25 wt%) to 90.1% (1.00 wt%)). The rate capabilities determined for the cells employing TMSi also supported this explanation (Fig. S3). More specifically, in the low C-rate charging/discharging process (<1.0 C), all cells exhibited similar specific discharge capacities because Li^+ migration between the electrodes was not seriously hindered under the slow charging/discharging environment. However, in the high C-rate charging/discharging process, the rate capabilities of the cells appeared to depend on the amount of additive present in the electrolyte. In this case, the cell cycled with 0.25 wt% MTSi exhibited the highest capacity retention at 2.0 and 3.0 C, i.e., 97.1% and 95.2% specific capacity retention was recorded compared to the specific discharge capacity with charging at 0.1 C. The cell cycled with 0.50 wt% MTSi also showed a moderately retained rate performance (96.8% and 94.6% at 2.0 and 3.0 C, respectively), while the cell cycled with 1.00 wt% MTSi showed a decreased rate capability (95.0% and 91.1% at 2.0 and 3.0 C, respectively). It should also be noted that a trade-off effect exists between F^- scavenging and the electrochemical performances in the cell, whereby higher quantities of dissolved Si-additives effectively lower the F^- concentration in the cell due to scavenging, and this results in a decreased ionic conductivity for the electrolyte, ultimately resulting in cell fading. Furthermore, the use of low quantities of additives is beneficial to also reduce the costs associated with these LIBs.

Thus, based on the above results, the high temperature performances of the cells were investigated using electrolytes containing 0.25 wt% of additive. At high temperatures, the initial potential profiles were similar, and the initial specific capacities were maintained at ~107.8 mAh g^{-1}, similar to those cycled at room temperature (Fig. 3c and d). In terms of the cycling performance, the cell cycled with the standard electrolyte exhibited 92.7% retention, while the cells cycled with electrolytes containing MTSi, DDSi, and TMSi exhibited increased retention values of 93.8%, 94.3%, and 95.0%, respectively. Interestingly, the Si-based additives resulted in meaningful differences in their retention ratios of the graphite anode specific capacity (Fig. S4a). More specifically, the cells cycled with Si-additives exhibited improved cycling performances compared to that cycled with only the standard electrolyte (83.1%), whereby the cell cycled with MTSi revealed the highest

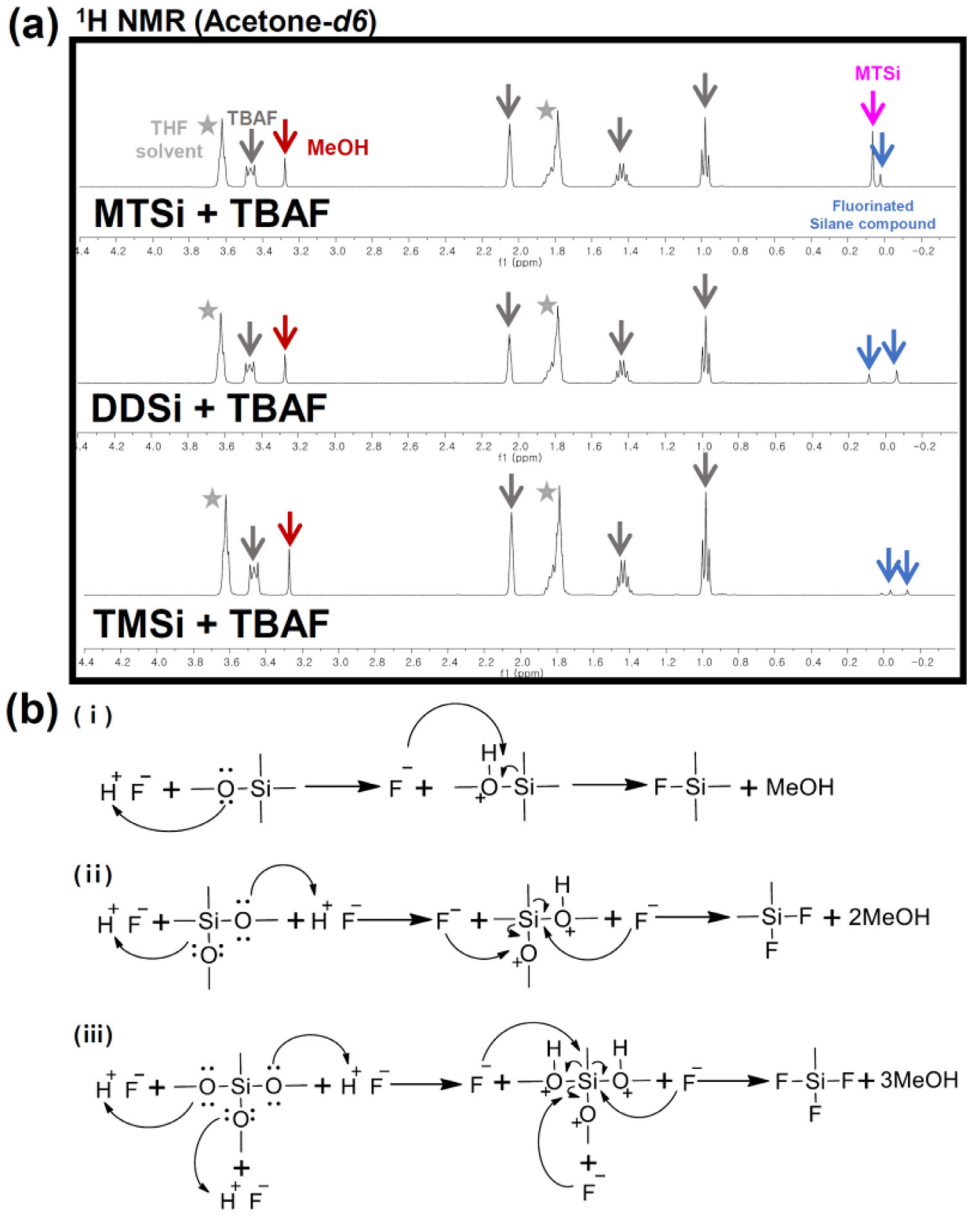

Fig. 2. (a) ^{1}H NMR spectra for solution after chemical reaction of MTSi, DDSi, and TMSi with TBAF, (b) mechanism of MTSi, DDSi, and TMSi for HF scavenging reaction.

specific capacity retention (98.2%) and the cells cycled with DDSi and TMSi showed improved specific capacity retentions (96.6% and 95.1%). Additional SEM analyses for the cycled graphite anode indicated that the graphite anode cycled with MTSi exhibited a relatively clean surface state, however, the surface of graphite anode cycled with TMSi appeared to be covered with chemical components potentially originating from electrolyte decomposition (Fig. S4b). These results indicate that MTSi appears to be the most effective additive for improving the cycling performances of LIBs.

Based on these observations, electrochemical evaluation of the Si-additives was performed at high temperatures using the LMO/graphite full-cell (Fig. 4). To determine the effectiveness of the Si-additive, it is important to examine the LMO/graphite full-cell performance since Mn corrosion not only accelerates the deformation of the LMO cathode, but also triggers rapid fading of the graphite anode, since the dissolved Mn significantly hinders the formation of a stable SEI layer on the anode surface [55,56]. In the present study, the cell cycled with the standard electrolyte exhibited a drastic decrease in the cell capacity, with only 64.4% of the capacity being observed after 100 cycles. In contrast, the cells cycled with the Si-additive-containing electrolytes exhibited improved cycling retention values, i.e., 71.0%, 69.1%, and 67.4% retention for the cells cycled with MTSi, DDSi, and TMSi, respectively, after 100 cycles. In terms of the average coulombic efficiencies, the cell cycled with 0.25 wt% MTSi, DDSi, and TMSi exhibited 99.6%, 99.5%, and 99.4% average coulombic efficiencies, while the cell cycled in the absence of Si-additives gave a corresponding value of 99.1%. These results indicate that use of Si-additives is effective for improving the cycling performances of full-cells.

To demonstrate the role of Si-additives in the cell, the surface morphologies of the cycled electrodes were analyzed by SEM and TEM (Fig. 5). In contrast to the pristine LMO cathode, numerous cracks were observed in the cycled LMO cathodes that contained no additives. Notably, when Mn corrosion occurs via a chemical reaction with the F^{-} species in the cell, it causes pulverization of the active material, as the particle strength decreases due to deformation of the cathode structure [57,58]. This indicates that in the LMO cathode cycled without additives, the Mn dissolution reaction

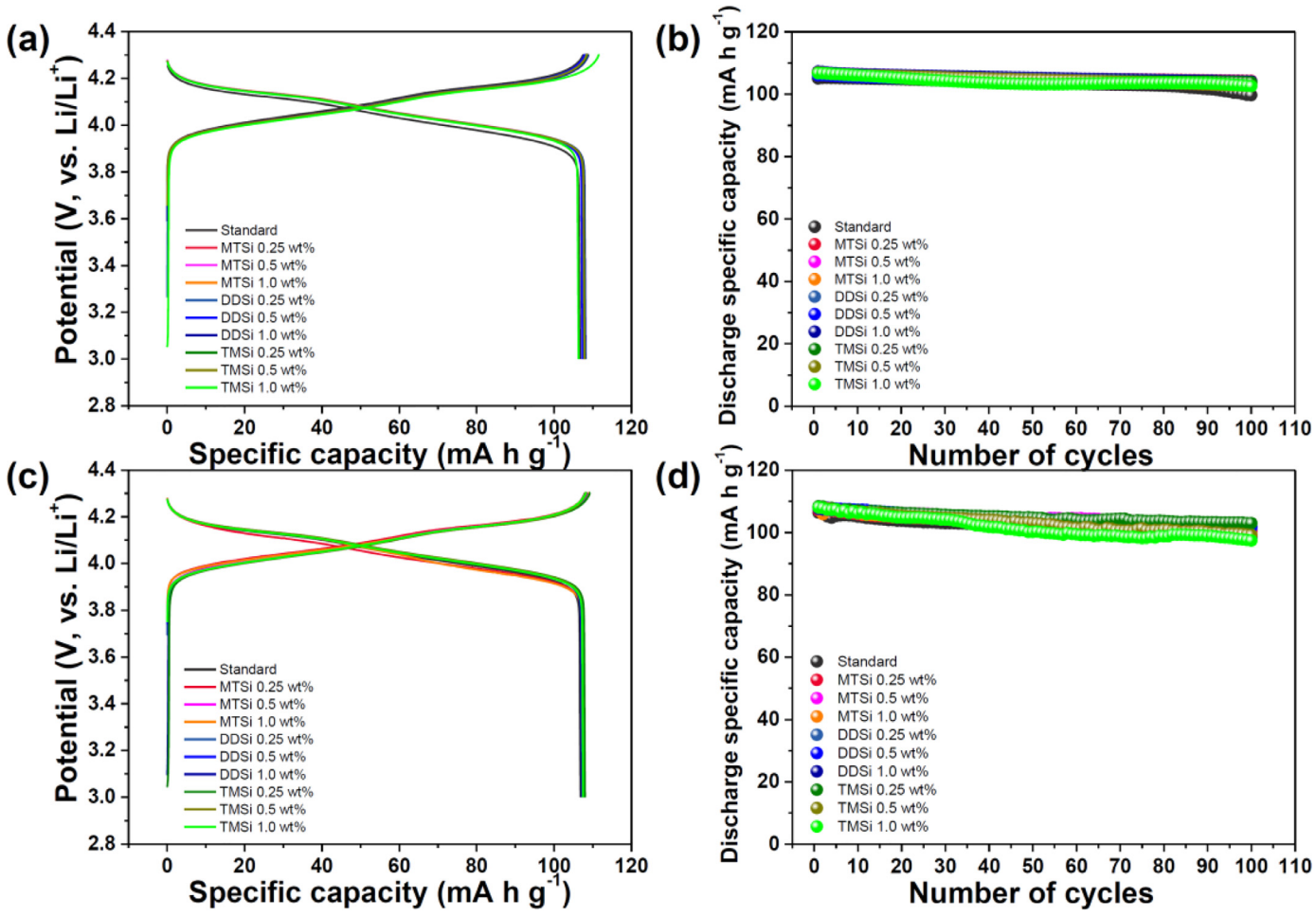

Fig. 3. Electrochemical performance of LMO half cells cycled with standard electrolyte (black), MTSi-containing electrolyte (red), DDSi-containing electrolyte (blue), and TMSi containing electrolyte (green): (a) potential profiles at 1 cycle at 25 °C, (b) cycling performances at 25 °C, (c) potential profiles at 1 cycle at 45 °C, and (d) cycling performances at 45 °C.

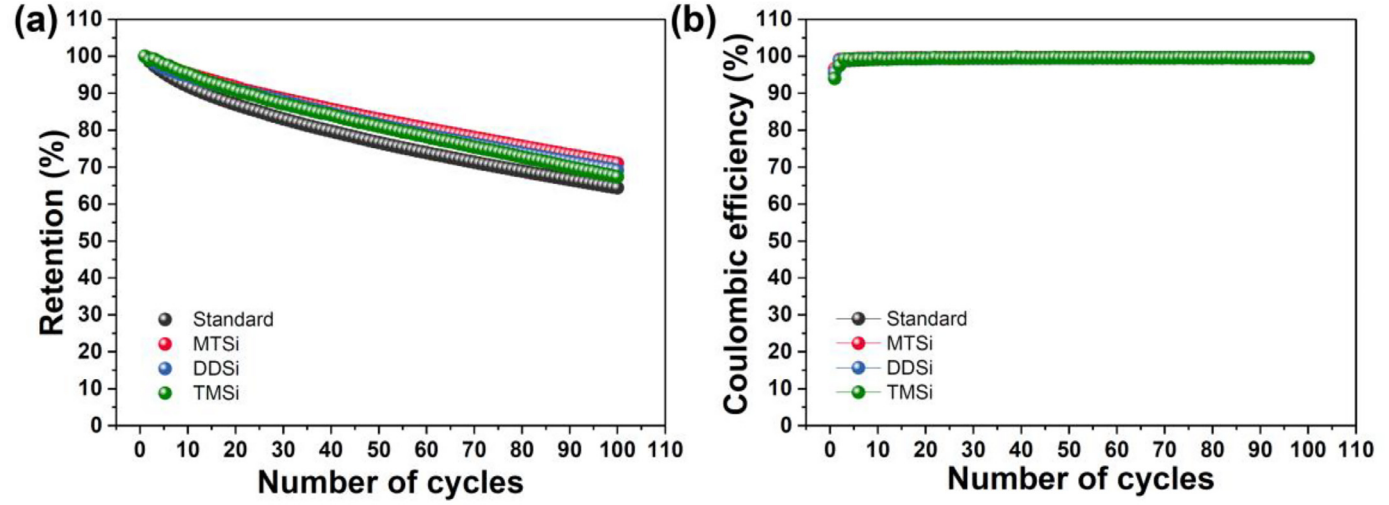

Fig. 4. Electrochemical performances of full-cell assembled with LMO/graphite cycled with standard electrolyte (black), MTSi-containing electrolyte (red), DDSi-containing electrolyte (blue), and TMSi containing electrolyte (green): (a) retention after 100 cycles at 45 °C, and (b) coulombic efficiency at 45 °C.

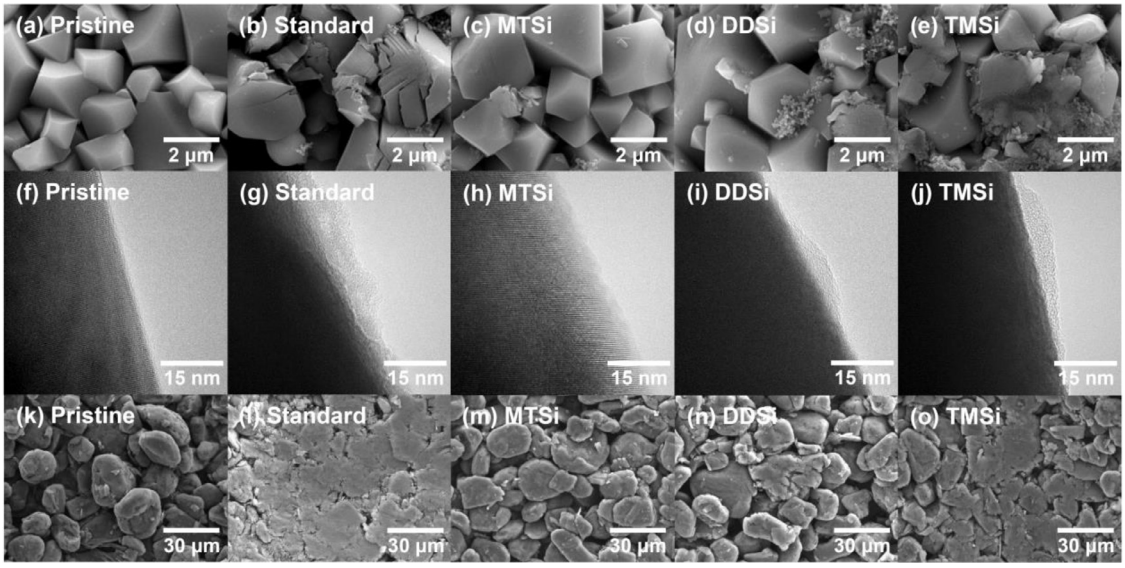

Fig. 5. SEM images of (a) pristine LMO electrode, and (b–e) recovered LMO electrodes cycled with standard electrolyte and Si-containing additives, TEM images of (f) pristine LMO electrode, and (g–j) recovered LMO electrodes cycled with standard electrolyte and Si-containing additives, SEM images of (k) pristine graphite electrode, and (l–o) recovered graphite electrodes cycled with standard electrolyte and Si-containing additives.

occurs in the cell, leading to cracks in the primary particles. In contrast, the cycled LMO cathode controlled by the MTSi-containing electrolyte exhibited a clean surface with negligible particle cracks, indicating that MTSi effectively removes the F^- species in the cell, resulting in an increase in the surface stability of the LMO cathode. Additional analysis of the particle strength of the cycled LMO cathode material strongly supports these observations (Fig. S5). More specifically, the pristine LMO cathode material (non-cycled) exhibited a particle strength of 750.2 MPa, which decreased significantly to 178.2 MPa upon electrochemical cycling. This suggests the occurrence of serious undesired reactions on the surface of the LMO cathode material, which affect the electrochemical performance. In contrast, the LMO cathode materials controlled by the Si-additive-containing electrolytes exhibit relatively improved particle strength values. Although TMSi resulted in a particle strength of only 213.4 MPa after cycling, the corresponding values for MTSi and DDSi were 484.2 and 461.5 MPa, respectively, thereby indicating that the undesired reactions were suppressed on the surface of the LMO cathode. As shown in Fig. 3, Si-additives exhibited similar retention ratios for the half-cell performances, implying that the differences in the particle strengths of the cycled LMO cathode materials may be due to another undesired reaction originating from the graphite anode. Indeed, previous studies have reported that when the electrolyte is decomposed at the electrolyte/electrode interface, the decomposed adducts can easily diffuse to both the cathode and the anode via dissolution in the electrolyte [59–61]. When these decomposed adducts reach cathode side, they can re-precipitate on the cathode surface by additional electrochemical decomposition, in addition to migrating into microcracks, thereby accelerating the reducing in particle strength of the cathode material [62–68]. Considering these recent studies, it could be considered that TMSi appears to decompose on the graphite surface, thereby affecting the particle strength of the LMO cathode material during the electrochemical process. The TEM results are also consistent with this observation. While the surface of the cycled LMO cathode controlled by the standard electrolyte was irregular and rough, relatively clean and smooth surfaces were observed for the cycled LMO cathodes controlled by the electrolytes containing Si-additives. In addition, the graphite anode cycled in the absence of additives was covered with a thick film, possibly due to electrolyte decomposition. This indicates that a stable SEI layer cannot be formed on the surface of the graphite anode because of Mn dissolution [69–72]. In contrast, the surface of the graphite anode controlled by an electrolyte containing an Si-additive was relatively clean, suggesting that these additives improve the surface stability of both the LMO cathode and the graphite anode, ultimately leading to an improved cycling retention of the cell.

Moreover, the EIS results also indicate that the Si-additives are effective in increasing the surface stability of the LMO cathode materials (Fig. 6). During the initial cycles, the overall internal resistances (R_{Inter}) were similar, and the R_{Inter} value of the MTSi-based cell was slightly higher than that of the cell cycled in the absence of Si-additives (17.1 Ω for the bare LMO and 20.1 Ω for MTSi-LMO). This observation can be attributed to the difference in the ionic conductivity of the electrolyte, since this dominates the kinetic behavior of the cell during the initial cycling [73,74]. However, the internal resistances were found to increase significantly in the cell cycled with the bare LMO cathode, whereby R_{Inter} and R_{CT} increase to 63.5 and 46.9 Ω, respectively, whereas the cell cycled with the MTSi additive exhibited R_{Inter} and R_{CT} values of 41.9 and 28.2 Ω, respectively. These results indicate that the use of MTSi considerably reduces the internal resistances of the cell because it effectively increases the surface stability of the unstable LMO cathode materials. Indeed, the XPS results provide spectroscopic evidence to support this observation (Fig. 7a). More specifically, in the C 1*s* spectra, the intensities of RC (=O)R (287.5 eV) [75], and –O–C=O (290.5 eV) [76,77] in the cycled bare LMO cathode are stronger than those for the cycled cathode containing the MTSi additive. Notably, these carbon species are indicative of electrolyte decomposition [78–80], and suggest that the undesired electrolyte decomposition readily occurs in the cell cycled with the bare LMO cathode. The F 1*s* and P 2*p* spectral data are also consistent with these results; the decomposed adducts of LiF (686.5 eV in the F 1*s* spectra) [81] and Li_xPF_y (687.9 eV in F 1*s* and 136.6 eV in P 2*p* spectra) [82,83] are present in significantly high quantities in the cycled bare LMO cathode, and therefore decrease the cycling performance of the cell. Notably, when electrolyte decomposition occurs in the cell, F^- species are formed, thereby triggering the dissolution of TM via a chemical reaction [84,85]. In this study, the dissolved Mn present on the graphite anode is considerably reduced in the cell cycled with the MTSi additive (208.4 ppm), whereas the cell cycled with the bare LMO cathode was found to contain 277.0 ppm of dissolved Mn on

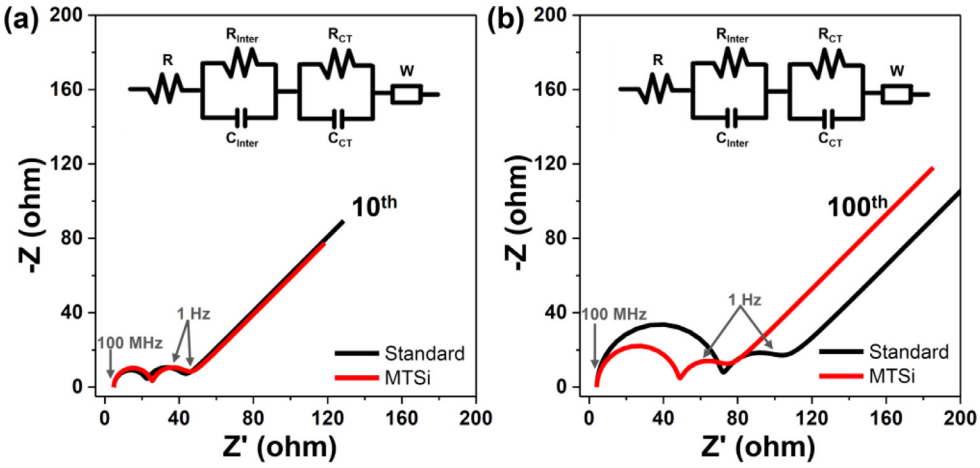

Fig. 6. EIS analysis of LMO electrode after (a) 10 cycles and (b) 100 cycles (black: standard electrolyte, red: MTSi-containing electrolyte).

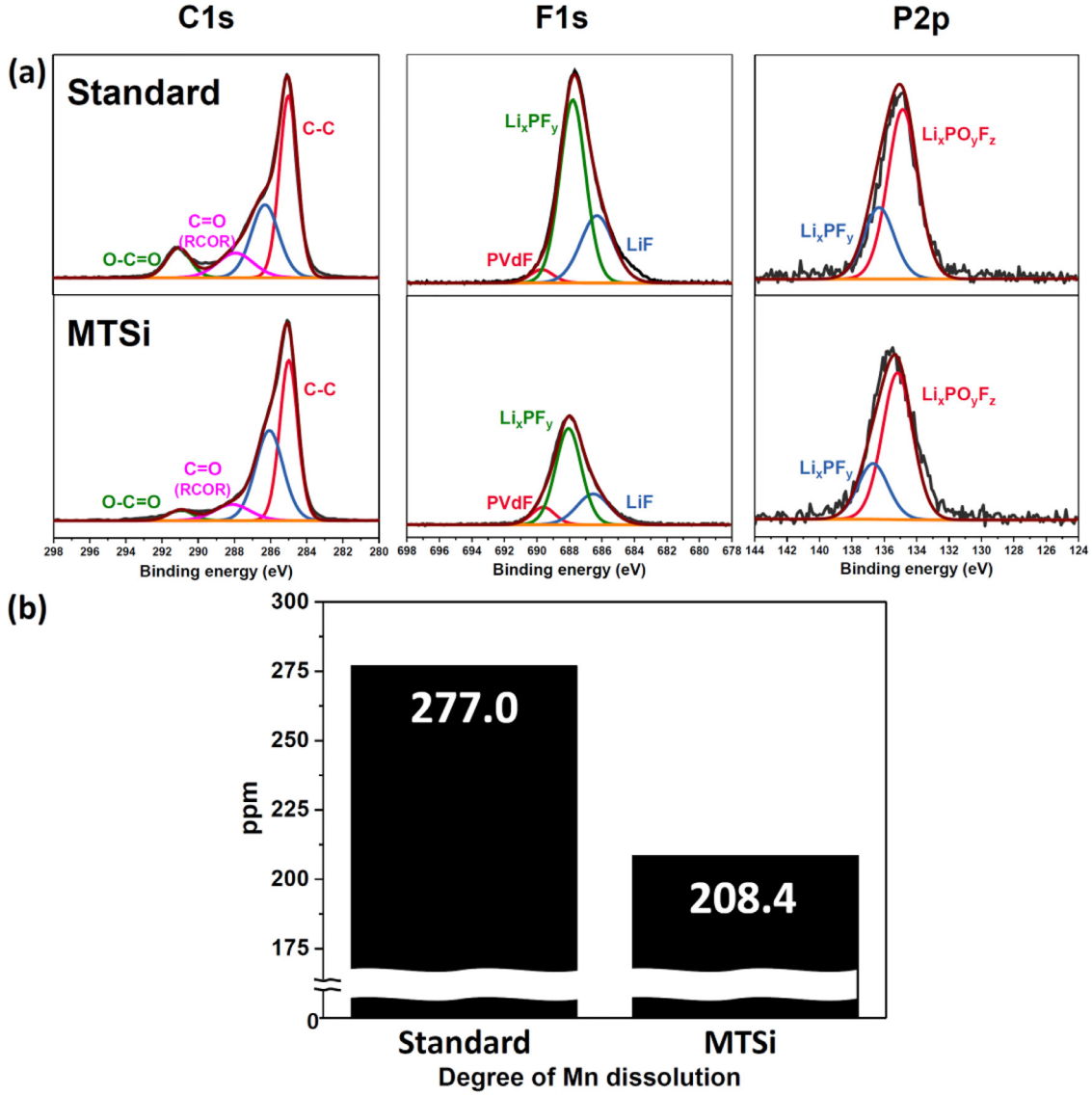

Fig. 7. (a) XPS spectra for cycled LMO electrodes, (b) quantitative analysis for formed Mn species on anode.

the graphite anode (Fig. 7b). Thus, the MTSi additive effectively suppresses Mn dissolution in the cell via the chemical scavenging reaction, thereby leading to an improved interfacial stability for the LMO cathode material even at high temperatures.

4. Conclusions

To suppress the severe Mn dissolution commonly observed in LMO cathodes, Si–O functionalized task-specific additives, namely MTSi, DDSi, and TMSi, were proposed. These additives were found to be effective in selectively scavenging the F^- species present in the cell, thereby resulting in a desirable chemical reactivity through Si–F bond formation, as demonstrated by ex-situ NMR analyses. As a result, the cells cycled in the presence of these Si-additives exhibited improved cycling retentions at room temperature and 45 °C. Among the various candidates, a combination of MTSi and the LMO cathode afforded the best results in terms of improving the electrochemical performances, such as the cycling retention (93.8% retention of the half-cell and 71.0% retention of the full-cell), whereas the cell cycled with the standard electrolyte exhibited fading of the cycling retention due to Mn dissolution (92.7% retention of the half-cell and 64.4% retention of the full-cell). Additional ex-situ analyses of the surfaces of the cycled electrodes showed that the use of MTSi not only improves the surface stability of the LMO cathode but also that of the graphite anode. Furthermore, the primary particles of the LMO cathodes cycled in the presence of MTSi were maintained, as Mn dissolution was effectively suppressed. Numerous cracks were also observed in the LMO cathodes cycled in the absence of MTSi, thereby indicating that Mn corrosion is significantly inhibited by the use of MTSi. Moreover, the surfaces of the graphite anodes cycled in the presence of MTSi were found to be clean and regular, whereas those cycled with the standard electrolyte were covered with decomposed adducts formed through electrolyte decomposition. It can therefore be concluded that MTSi is an effective candidate to delay or mitigate the deformation of LMO cathode materials in cell, and so can be employed to build more efficient LIBs.

Declaration of competing interests

The authors declare that they have no known competing financial interests or personal relationships that could have appeared to influence the work reported in this paper.

Acknowledgments

This work was supported by National Research Foundation of Korea grant from the Korean government (MSIP) (NRF-2019R1C1C1002249, and NRF-2017M1A2A2044506).

Supplementary materials

Supplementary material associated with this article can be found, in the online version, at doi:10.1016/j.jechem.2020.02.029.

References

[1] B. Scrosati, J. Hassoun, Y.-K. Sun, Energy Environ. Sci. 4 (2011) 3287–3295.
[2] J.W. Fergus, J. Power Sour. 195 (2010) 939–954.
[3] A. Yoshino, Angew. Chem. Int. Ed. 51 (2012) 5798–5800.
[4] J. Hassoun, P. Reale, B. Scrosati, J. Mater. Chem. 17 (2007) 3668–3677.
[5] M.S. Whittingham, MRS Bull. 33 (2008) 411–419.
[6] A. Patil, V. Patil, D.W. Shin, J.-W. Choi, D.-S. Paik, S.-J. Yoon, Mater. Res. Bull. 43 (2008) 1913–1942.
[7] K. Fu, Z. Wang, C. Yan, Z. Liu, Y. Yao, J. Dai, E. Hitz, Y. Wang, W. Luo, Y. Chen, M. Kim, L. Hu, Adv. Energy Mater. 6 (2016) 1502496.
[8] Y. Liu, J. Wang, J. Wu, Z. Ding, P. Yao, S. Zhang, Y. Chen, Adv. Energy Mater. (2019) 1903139.
[9] G.Q. Liu, H.T. Kuo, R.S. Liu, C.H. Shen, D.S. Shy, X.K. Xing, J.M. Chen, J. Alloys Compd. 496 (2010) 512–516.
[10] X. Wang, X. Zheng, Y. Liao, Q. Huang, L. Xing, M. Xu, W. Li, J. Power Sour. 338 (2017) 108–116.
[11] T. Ohzuku, A. Veda, M. Nagayama, Y. Iwakoshi, H. Komori, Electrochim. Acta 38 (1993) 1159–1167.
[12] M. Broussely, P. Biensan, B. Simon, Electrochim. Acta 45 (1999) 3–22.
[13] S.-T. Myung, F. Maglia, K.-J. Park, C.S. Yoon, P. Lamp, S.-J. Kim, Y.-K. Sun, ACS Energy Lett. 2 (2017) 196–223.
[14] S. Neudeck, F. Walther, T. Bergfeldt, C. Suchomski, M. Rohnke, P. Hartmann, J. Janek, T. Brezesinski, ACS Appl. Mater. Interf. 10 (2018) 20487–20498.
[15] T. Yim, K.S. Kang, J. Mun, S.H. Lim, S.-G. Woo, K.J. Kim, M.-S. Park, W. Cho, J.H. Song, Y.-K. Han, J. Power Sour. 302 (2016) 431–438.
[16] S. Liu, L. Xiong, C. He, J. Power Sour. 261 (2014) 285–291.
[17] D.-W. Jun, C.S. Yoon, U.-H. Kim, Y.-K. Sun, Chem. Mater. 29 (2017) 5048–5052.
[18] D.K. Kim, P. Muralidharan, H.-W. Lee, R. Ruffo, Y. Yang, C.K. Chan, H. Peng, R.A. Huggins, Y. Cui, Nano Lett. 8 (2008) 3948–3952.
[19] Y.L. Ding, J. Xie, G.S. Cao, T.J. Zhu, H.M. Yu, X.B. Zhao, J. Phys. Chem. C 115 (2011) 9821–9825.
[20] K.H. Jung, H.G. Kim, Y.J. Park, J. Alloys Compd. 509 (2011) 4426–4432.
[21] I. Belharouak, Y.-K. Sun, W. Lu, K. Amine, J. Electrochem Soc. 154 (2007) A1083–A1087.
[22] R. Wang, S. Xiao, X. Li, J. Wang, H. Guo, F. Zhong, J. Alloys Compd. 575 (2013) 268–272.
[23] C.-K. Kim, D.–S. Shin, K.–E. Kim, K. Shin, J.–J. Woo, S. Kim, S.Y. Hong, N.–S. Choi, Chem. Electro. Chem. 3 (2016) 913–921.
[24] Z.H. Lu, D.D. MacNeil, J.R. Dahn, Electrochem. Solid-State Lett. 4 (2001) A200–A203.
[25] M.M. Thackeray, S.H. Kang, C.S. Johnson, J.T. Vaughey, R. Benedek, S.A. Hackney, J. Mater. Chem. 17 (2007) 3112–3125.
[26] D. Aurbach, A. Zaban, Y. Ein-Eli, I. Weissman, O. Chusid, M. Levi, E. Levi, A. Schechter, E. Granot, J. Power Sour. 68 (1997) 91–98.
[27] S.F. Lux, I.T. Lucas, E. Pollak, S. Passerini, M. Winter, R. Kostecki, Electrochem. Commun. 14 (2012) 47–50.
[28] Y. Okamoto, J. Electrochem. Soc. 160 (2013) A404–A409.
[29] H. Wang, W. Ge, F. Wang, W. Liu, M.-Z. Qu, G. Peng, ACS Appl. Mater. Interf. 8 (2016) 18439–18449.
[30] A.Francis Carey, R.J. Sundberg, Advanced Organic Chemistry Part A: Structure and Mechanisms, fifth ed., Springer, Germany, 2006.
[31] K.J. Gruntz, L. Ley, R.L. Johnson, Phys. Rev. B 24 (1981) 2069–2080.
[32] V. Etacheri, R. Marom, R. Elazari, G. Salitra, D. Aurbach, Energy Environ. Sci. 4 (2011) 3243–3262.
[33] O.K. Park, Y. Cho, S. Lee, H.-C. Yoo, H.-K. Song, Energy Environ. Sci. 4 (2011) 1621–1633.
[34] T.-J. Kim, D. Son, J. Cho, B. Park, J. Power Sour. 154 (2006) 268–272.
[35] S.B. Park, S.M. Lee, H.C. Shin, W.I. Cho, H. Jang, J. Power Sour. 166 (2007) 219–225.
[36] T. Inoue, M. Sano, J. Electrochem. Soc. 145 (1998) 3704–3707.
[37] T. Aoshima, K. Okahara, C. Kiyohara, K. Shizuka, J. Power Sour. 97-98 (2001) 377–380.
[38] S.S. Zhang, J. Power Sour. 162 (2006) 1379–1394.
[39] K. Nagajima, Y. Nishi, T. Osaka, M. Datta (Eds.), Energy Storage Systems for Electronics, Gordon and Breach Science Publisher, Singapore, 2000.
[40] J. Barthel, H.J. Gores, J.O. Besenhard (Eds.), Handbook for Battery Materials, Wiley-VCH, Weinheim, 1999.
[41] T. Sato, T. Maruo, S. Marukane, K. Takagi, J. Power Sour. 138 (2004) 253–261.
[42] M. Wakihara, Mater. Sci. Eng. R Rep. 33 (2001) 109–134.
[43] C. Blondel, C. Delsart, F. Goldfarb, J. Phys. B 34 (2001) L281–L288.
[44] R.K. Sharma, J.L. Fry, J. Org. Chem. 48 (1983) 2112–2114.
[45] A.S. Pilcher, H.L. Ammon, P. DeShong, J. Am. Chem. Soc. 117 (1995) 5166–5167.
[46] V.Kotlyar H.E.Gottlieb, A. Nudelman, J. Org. Chem. 62 (1997) 7512–7515.
[47] Y. Paik, S. -S. Kim, O.H. Han, Angew. Chem. Int. Ed. 47 (2008) 94–96.
[48] O.H. Han, K.S. Han, C.W. Shin, J. Lee, S. -S. Kim, M.S. Um, H. -I. Joh, S. -K. Kim, H.Y. Ha, Angew. Chem. Int. Ed. 47 (2012) 3842–3845.
[49] S.H. Jang, T. Yim, Chem. Phys. Chem. 18 (2017) 1–6.
[50] G.A. Olah, L. Heiliger, X.-Y. Li, G.K.S. Prakash, J. Am. Chem. Soc. 112 (1990) 5991–5995.
[51] S.H. Jang, K.–J. Lee, J. Mun, Y.–K. Han, T. Yim, J. Power Sour. (2019) 15–24 410-411.
[52] J.W. Emsley, J. Feeney, L.H. Sutcliffe, High Resolution Nuclear Magnetic Resonance Spectroscopy, second ed., Pergamon Press, London, 1968.
[53] P. Murray-Rust, J.P. Glusker, J. Am. Chem. Soc. 106 (1984) 1018–1025.
[54] A.A. Macharashvili, V.E. Shklover, Yu.T. Struchkov, G.I. Oleneva, E.P. Kramarova, A.G. Shipov, Y.I. Baukov, J. Chem. Soc. Chem. Commun. (1988) 683–685.
[55] H. Tsunekawa, S. Tanimoto, R. Marubayashi, M. Fujita, K. Kifune, M. Sano, J. Electrochem. Soc. 49 (2002) A1326–A1331.
[56] I.H. Cho, S.-S. Kim, S.C. Shin, N.-S. Choi, Electrochem. Solid-State Lett. 13 (2010) A168–A172.
[57] H. Yamane, T. Inoue, M. Fujita, M. Sano, J. Power Sour. 99 (2001) 60–65.
[58] A. Blyr, A.D. Pasquier, G. Amatucci, J.-M. Tarascon, Ionics (Kiel) 3 (1997) 321–331.
[59] S. Fang, D. Jackson, M.L. Dreibelbis, T.F. Kuech, R.J. Hamers, J. Power Sour. 373 (2018) 184–192.
[60] Y.S. J.ung, P. Lu, A.S. Cavanagh, C. Ban, G.-H Kim, S.-H Lee, S.M. George, S.J. Harris, A.C. Dillon, Adv. Energy Mater. 3 (2013) 213–219.
[61] D. Aurbach, J. Power Sour. 80 (2000) 206–218.

[62] Y. Hu, X. Zhao, Z. Suoa, J. Mater. Res. 25 (2010) 1007–1010.
[63] J.H. S.ong, Y.J. Kim, J. Kim, S.M. Oh, S. Yoon, Bull. Korean Chem. Soc. 37 (2016) 1298–1304.
[64] P. Yan, J. Zheng, M. Gu1, J. Xiao, J.–G. Zhang, C.–M. Wang, Nat. Commun. 8 (2017) 14101 8.
[65] B. Xiao, X. Sun, Adv. Energy Mater. 8 (2018) 1802057.
[66] S. Hashigami, Y. Kato, K. Yoshimi, H. Yoshida, T. Inagaki, M. Hashinokuch, T. Doi, M. Inaba, Electrochim. Acta 29 (2018) 304–310.
[67] W. Cho, J.H. Song, K.–W. Lee, M.–W. Lee, H. Kim, J.–S. Yu, Y.–J. Kim, K.J. Kim, J. Phys. Chem. Solids 123 (2018) 271–278.
[68] R. Deshpande, M. Verbrugge, -T.Cheng Y, J. Wang, P. Liu, J. Electrochem. Soc. 159 (2012) A1730–A1738.
[69] M.-H. Ryou, G.-B. Han, Y.M. Lee, J.-N. Lee, D.J. Lee, Y.O. Yoon, J.-K. Park, Electrochim. Acta 55 (2010) 2073–2077.
[70] S. Komaba, B. Kaplan, T. Ohtsuka, Y. Kataoka, N. Kumagai, H. Groult, J. Power Sour. 119–121 (2003) 378–382.
[71] S. Komaba, T. Itabashi, T. Ohtsuka, H. Groult, N. Kumagai, B. Kaplan, H. Yashiro, J. Electrochem. Soc. 152 (2005) A937–A946.
[72] T. Sasaki, T. Abe, Y. Iriyama, M. Inaba, Z. Ogumi, J. Power Sour. 150 (2005) 208–215.
[73] S. Menne, J. Pires, M. Anouti, A. Balducci, Electrochem. Commun. 31 (2013) 39–41.
[74] X. Wang, W. Zheng, Y. Liao, Q. Huang, L. Xing, M. Xu, W. Li, J. Power Sour. 338 (2017) 108–116.
[75] M. Khan, A.H. Al-Marri, M. Khan, M.R. Shaik, N. Mohri, S.F. Adil, M. Kuniyil, H.Z. Alkhathlan, A. Al-Warthan, W. Tremel, M.N. Tahir, M.R.H Siddiqui, Nanoscale Res. Lett. 10 (2015) 281–289.
[76] E. Aliyev, V. Filiz, M.M. Khan, Y.J. Lee, C. Abetz, V. Abetz, Nanomaterials 9 (2019) 1180–1194.
[77] S.J. An, J. Li, C. Daniel, D. Mohanty, S. Naqpure, D. L. W. III, Carbon N Y 105 (2016) 52–76.
[78] D. Aurbach, Y. Ein-Ely, A. Zaban, J. Electrochem. Soc. 141 (1994) L1–L3.
[79] B. Ravdel, K.M. Abraham, R. Gitzendanner, J. DiCarlo, B. Lucht, C. Campion, J. Power Sour. 119-121 (2003) 805–810.
[80] D. Bar-Tow, E. Peled, L. Burstein, J. Electrochem. Soc. 146 (1999) 824–832.
[81] B. Deng, H. Wang, W. Ge, X. Li, X. Yan, T. Chen, M. Qu, G. Peng, Electrochim. Acta 236 (2017) 61–71.
[82] D. Ensling, M. Stjerndahl, A. Nyten, T. Gustafsson, J.O. Thomas, J. Mater. Chem. 19 (2009) 82–88.
[83] A.D. Pasquier, A. Blyr, P. Courjal, D. Larcher, G. Amatucci, B. Gérand, J.-M. Tarascon, J. Electrochem. Soc. 146 (1999) 428–436.
[84] J.-Y. Eom, I.-H. Jung, J.-H. Lee, J. Power Sour. 196 (2011) 9810–9814.
[85] B. Markovsky, A. Rodkin, G. Salitra, Y. Talyosef, D. Aurbach, H.-J. Kim, J. Electrochem. Soc. 151 (2004) A1068–A1076.